Korean J. Chem. Eng., 33(10), 2820-2829 (2016)
DOI: 10.1007/s11814-016-0188-1

pISSN: 0256-1115
eISSN: 1975-7220

Modeling of low viscosity oil-water annular flow in horizontal and slightly inclined pipes: Experiments and CFD simulations

Yi-Xin Pan*,†, Hong-Bing Zhang*, Rong-Hua Xie, Xing-Bin Liu**, and Min Wang****

*Department of Earth Science and Engineering, Hohai University, Nanjing 210098, China
**Daqing Oilfield, Daqing Logging & Testing Serv Co., Daqing 163453, China
(*Received 12 October 2015 • accepted 30 June 2016*)

Abstract−To characterize the effect of pipe inclination, low viscosity, flow rate and inlet water cut on annular flow pattern, a low viscosity oil-water two-phase annular flow in horizontal and slightly inclined (+1°, +3° and +5°) pipes with diameter of 20 mm has been experimentally investigated. A modified VOF model based on the CFD software package FLUENT was used to predict the in-situ oil fraction and pressure drop. The experimental data indicate that annular flow appears at a medium-high water cut. The slip ratio increases with flow rate increase but decreases with increasing water cut. The changes are more significant as the degree of inclination increases. Pressure drop is strongly dependent on flow rate, as it increases rapidly as inlet flow rate increase. Good agreement between the experimental data and calculated results of slip ratio and pressure drop was obtained.

Keywords: Oil-water Annular Flow, Inclined Pipe, Low Viscosity, Pressure Drop

INTRODUCTION

The instance of two immiscible fluids simultaneously flowing is common in the petroleum and chemical industries. For instance, oil and water are produced as a mixture from a wellbore and transported over long distances in modern oil fields. It is known that the two-phase flowing in pipes can form different flow regimes, which has been studied by many researchers [1-8] who have indicated that the physical properties of the fluids influenced the flow regimes. In addition, inclination angle is another parameter that affects the flow regimes [9-11].

The reduction of the pressure gradient in an oil-water two-phase flow for transportation in a well bore is significant in increasing the pumping efficiency or the production rate. Of all the flow regimes, annular flow, in which the oil is surrounded by water, has been given the most attention because the frictional pressure drop is approximate to that of water flowing alone under equivalent flow conditions. Ooms [12] analyzed the hydrodynamic stability of core annular flow (CAF) base on the hypothesis of the two phase idea. Oliemans and Ooms [13] presented a lubricating-film model to predict the CAF pressure reduction. Arney et al. [14] obtained a formula to estimate the CAF holdup fraction based on boundaries from experimental data. Bai et al. [15] numerically investigated the spatially periodic wave core flows of an oil-water two-phase with the same density and high viscosity ratio. In the following decade, a body of theoretical and experimental research on the CAF was presented. The challenge of heavy oil transport lubricated by water was summarized by Joseph et al. [16].

An annular flow regime is influenced by many aspects, such as fluid properties and pipe geometry. In addition, the stability of the flow regime is also affected by these factors and a large body of research data is available on these aspects [12,17-19]. The physics between the two phases and shape influence the stability of core-annular flow, and effects from interfacial wave was negligible [20-22]. In addition, at different pipeline inclinations the velocity required to form the annular flow changed. Strazza et al. [23] reported that in keeping the superficial water velocity constant, the oil velocity required for annular flow increased as the pipeline inclination increased; thus, the region of annular flow was reduced as the inclined angle increased. The majority of research data available in the literature on annular flow is based on the high viscosity ratio [20,22, 23]; notably few studied low viscosity ratio for annular flow [8].

However, several investigations for the simulation of annular flow have been reported [15,24-27]. Among these, Bai et al. [15] simulated an axisymmetric equal density core flow. The wavy core flow was numerically simulated by Ko et al. [24], who presented the results of pressure gradient, velocity profile and pressure in turbulent flow. Ghosh et al. [25] simulated the flow of high viscous oil lubricated by water using the CFD software package FLUENT. Kaushik et al. [26] and McCaslin and Desjardins [27] numerically investigated the annular flow using the VOF model in the FLUENT software package.

Our aim was to study the low viscosity oil-water two-phase annular flow in horizontal and slightly upward-angled acrylic pipes experimentally and validate the results by numerical simulation using FLUENT 14.5. The pressure drop, in situ volumetric fraction, and flow images of the annular flow at different inclinations were obtained at various inputs of velocity and water cut.

EXPERIMENTAL PROCEDURE

The experimental studies on annular flow were executed in the

†To whom correspondence should be addressed.
E-mail: yxpan@hhu.edu.cn

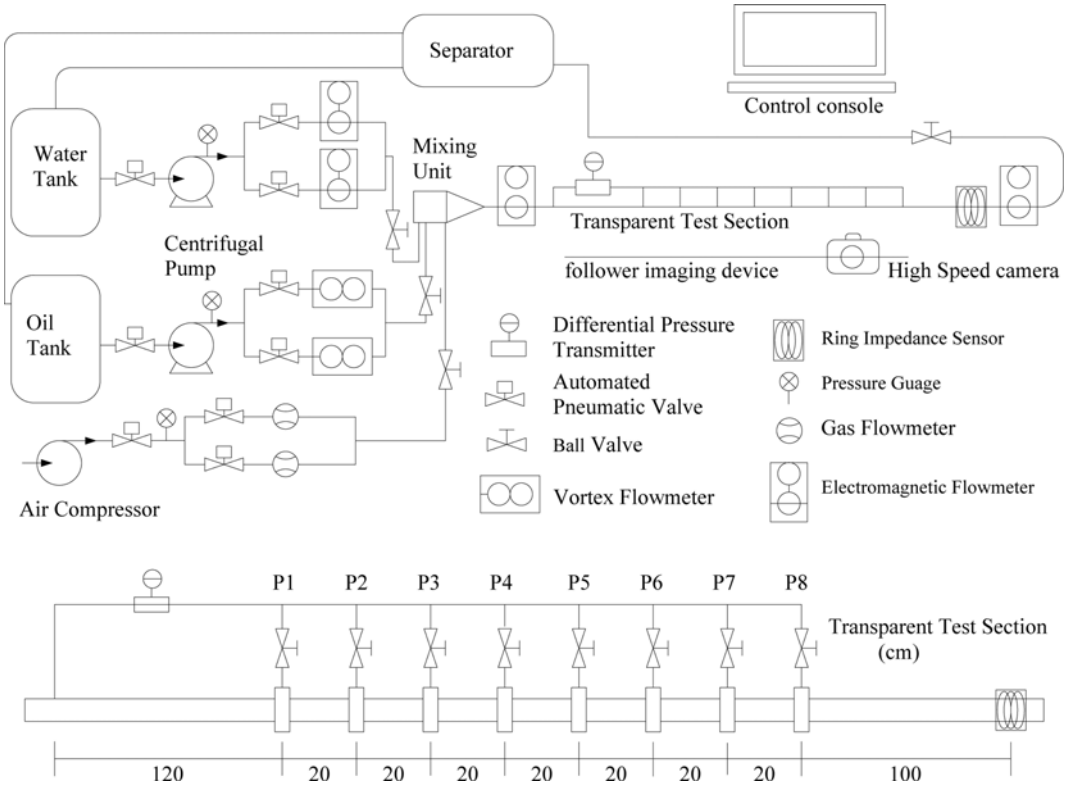

Fig. 1. The experimental schematic.

gas-oil-water pilot scale multiphase flow facility at Daqing Oilfield Limited Company, China. The experimental schematic diagram is depicted in Fig. 1. The multiphase flow system consists of three main components: a supply loop control, a test segment, and the observation and measurement system. Gas is pumped by a compressor and measured by a gas flow meter with an accuracy of 1% to full scale and a range of 0.7 to 7 m^3/h; the oil and water are supplied from their own tanks by using a pump and are measured by a vortex flow meter and an electromagnetic flow meter with the accuracy of 1% and 0.2% and range of 0.8 to 8 m^3/h and 0.3 to 13 m^3/h, respectively. The pressure drop was measured by differential pressure transducer with an accuracy of 0.5% that was connected to eight measuring points (P1-P8) at a spacing of 0.2 m in the test section and can be measured separately.

An acrylic test section with a length of 3.6 m and diameter (ID) of 20 mm was connected to the mixing unit and fixed to a steel beam that could adjust the pipeline inclination from 0° to +90°. The mixing unit was stainless steel and funnel-shaped (Fig. 2), with a 125 mm I.D. at one end and 20 mm at the other. The mixing unit, designed as a funnel, was used to mimic the flow characteristics of an actual flow in the horizontal well production profile test, and applied to a collecting umbrella, which is different from the structure designed to form an annular flow mixer [23]. The diameter of the oil and water inlet is 40 mm and the gas inlet is 10 mm; all inlets were connected to flexible pipe in order to be able to rotate with the test pipeline. In this study, the gas loop was closed, and oil and water loops were opened to study the oil-water two-phase annular flow.

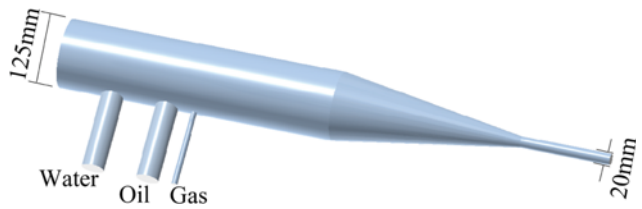

Fig. 2. The mixing unit.

A high speed camera system was used to record the annular flow structures, which consists of a SpeedCam MacroVis EoSens high speed camera made by HSVISION Company in Germany and a track follower. The camera can record 5,000 fps at the maximum resolution of 512×512. In this study, 500 fps and 1,200×800 pixels were chosen to analyze the annular flow characteristics. The camera can be moved automatically on the follower imaging device between the two electromagnetic flowmeters. Low viscous oil (No. 15 industry white oil with a density of 856 kg/m^3, viscosity of 12 mPa·s and surface tension of 35 mN/m) and tap water were used as test fluids.

MATHEMATICAL MODEL

There are three different models available in FLUENT for the simulation of multiphase flow. Among them, the volume of fluid (VOF) can model two or more immiscible fluids by solving a single set of momentum equations and tracking the volume fraction of each of the fluids throughout the domain. The VOF model is

widely used to simulate separated flow, annular flow [26,28-30] and stratified flow [31,32]. The equation for conservation of mass can be written as follows:

$$\frac{\partial \rho}{\partial t} + \mathbf{u} \cdot \nabla \rho = 0 \tag{1}$$

where **u** is the fluid velocity, and ρ is the fluid density. The Navier-Stokes momentum equation written as

$$\frac{\partial \rho \mathbf{u}}{\partial t} + \nabla \cdot (\mathbf{u} \cdot \mathbf{u}) = -\nabla p + \nabla \cdot [\mu(\nabla \mathbf{u} + \nabla \mathbf{u}^T)] + \rho \mathbf{g} \sin\theta + \mathbf{F}_{SF} \tag{2}$$

where p is the pressure, **g** is the gravitational acceleration and **F** is the body force; θ is the pipeline inclination angle. The term of (ρ**g**sinθ) is the gravity component perpendicular to flow direction, which is neglected in this study. The fluid properties of density and viscosity in the above equations are calculated as

$$f = \sum_{i=1}^{2} f_i \beta_i \tag{3}$$

where f presents density or viscosity, β is the phase fraction and $\Sigma\beta_i$=1

The continuum surface force (CSF) model [33] is used to calculate the surface tension across the oil-water interface, ($\mathbf{F}_{SF}$):

$$\mathbf{F}_{SF} = 2c_o \sigma \kappa \mathbf{n} \tag{4}$$

where σ is the surface tension, κ is the local surface curvature given by $\kappa = \nabla \cdot \hat{n}$ and $\hat{n} = n/|n|$, and n is the normal vector to the surface, defined in terms of c_o, $n = \nabla c_o$.

In k-ε turbulence models, the standard k-ε formulation is the most widely used model in CFD simulation of two-phase flow. This model is based on transport equations for turbulence of the kinetic energy, k, and its dissipation rate, ε [22,29,34]. However, the turbulent flow in the standard k-ε model is assumed to be fully developed and the effects of molecular viscosity are negligible. In the present study, the Reynolds number, Re ranged between 350 and 22000; therefore, the RNG k-ε turbulence model, which can account for low-Reynolds number effects, was selected to calculate turbulent viscosity flow. The RNG k-ε model is derived using a rigorous mathematical technique to improve the accuracy. Ghorai and Nigam [31] studied the gas-liquid flow numerically using the VOF model combined with the RNG k-ε turbulence model. Masood and Delgado [35] investigated flow hydrodynamics in bubble columns by employing an explicit algebraic Reynolds and RNG k-ε model. For the present study, the RNG model is given as

$$\frac{\partial (\rho k)}{\partial t} + \nabla \cdot (\rho k \mathbf{u}) = \nabla (\lambda_k \mu_{eff} \nabla k) + G_k - \rho \varepsilon \tag{5}$$

$$\frac{\partial (\rho \varepsilon)}{\partial t} + \nabla \cdot (\rho \varepsilon \mathbf{u}) = \nabla (\lambda_\varepsilon \mu_{eff} \nabla \varepsilon) + \frac{\varepsilon}{k}(C_{1\varepsilon} G_k - C_{2\varepsilon} \rho \varepsilon) - R_\varepsilon \tag{6}$$

$$G_k = \mu_t S^2 \tag{7}$$

$$S = \sqrt{2 S_{ij} S_{ij}} \tag{8}$$

where $C_{1\varepsilon}$ and $C_{2\varepsilon}$ are the constants of the RNG formulation with values of 1.42 and 1.68, respectively. λ is the inverse effective Prandtl number computed as follows:

$$\left|\frac{\lambda - 1.3929}{\lambda_0 - 1.3929}\right|^{0.6321} \left|\frac{\lambda + 2.3929}{\lambda_0 + 2.3929}\right|^{0.3679} = \frac{\mu}{\mu_{eff}} \tag{9}$$

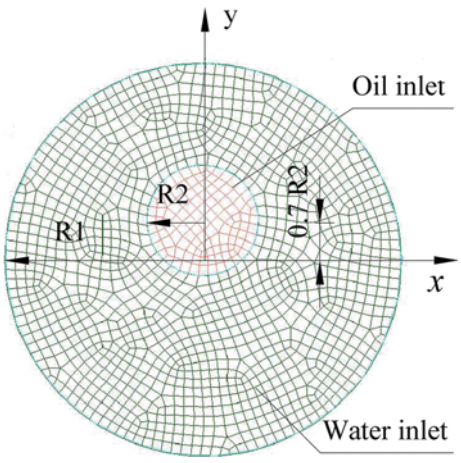

Fig. 3. The geometry and mesh of inlet.

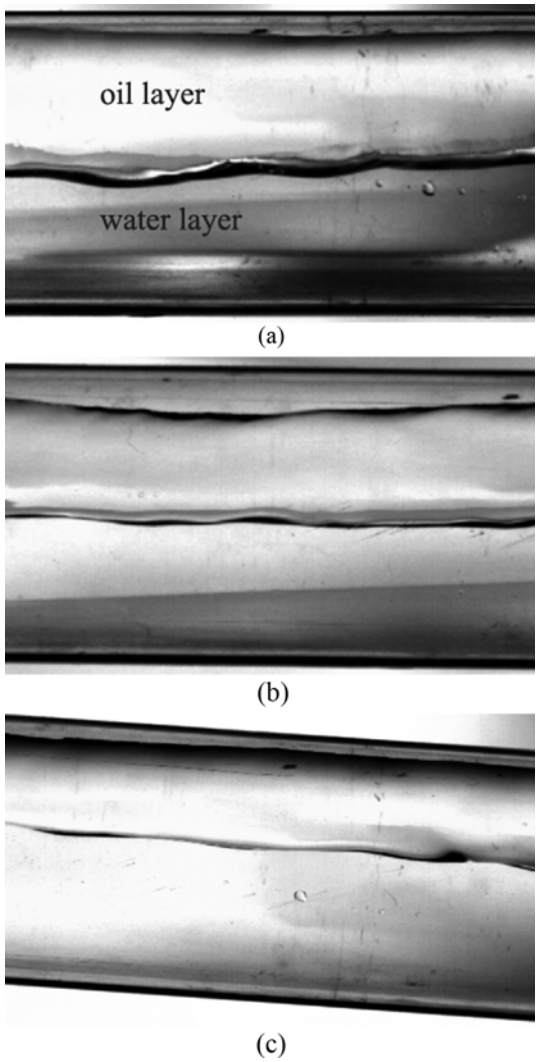

Fig. 4. The annular flow pattern at Q_m=15 m³/d in (a) θ=0°, (b) θ=+1° and (c) θ=+3° pipe.

where λ_0=1.0. μ_{eff} is the effective viscosity taken as $\mu_{eff}=\mu+\mu_t$. μ_t is the turbulent viscosity taken as $\mu_t=\rho C_\mu(k^2/\varepsilon)$ with C_μ=0.0845. The additional term in the RNG formulation compared with standard k-ε models is R_ε, which is given as

$$R_\varepsilon=\frac{C_\mu\rho\eta^3(1-\eta/\eta_0)}{1+\varphi\eta^3}\frac{\varepsilon^2}{k} \tag{10}$$

where φ=0.012, η_0=4.38, and η is defined as

$$\eta=S\frac{k}{\varepsilon}=\frac{k}{\varepsilon}\sqrt{\frac{G_k}{\mu_t}} \tag{11}$$

Three methods (mixture, dispersed and per-phase) of modeling turbulence in multiphase flows are available in FLUENT depending on the influence of the secondary phases. The k-ε mixture model is applicable when phases separate for stratified multiphase flows and when the density ratio between phases is close to 1. In the VOF model, the oil and water are dealt with as a mixture phase; meanwhile, in the present study, oil-water was a separate flow and the density ratio was close to 1. Thus, the k-ε mixture model was applied in this simulation.

The computational domain is a tube of 0.02 m in diameter and 1.0 m in length with two inlets and one outlet. The geometry is meshed by the software Gambit 2.4.6, and the inlet is illustrated in Fig. 3. For getting stable and converging solutions, grid independence was carried out with three different grids. The results show that the grid consisted of 253,941 independent cells for the simulation. To obtain the oil holdup with high precision, denser grids were used. It is sufficient to choose the grids numbered between 1,045,398 and 1,183,954 for different water cuts. A time step of 0.005 s and 0.01 s for the highest and lowest flow rate was selected to maintain stability. The mesh density used in this study is greater than the one obtained by Ghosh et al. [29] and Jiang et al. [30].

Uniform velocity distribution is assumed at the inlet boundary. At the oil inlet only oil is input and at the water inlet only water is input; therefore, $\mathbf{u}_o=\mathbf{u}_w=\mathbf{u}_z$ and $\mathbf{u}_x=\mathbf{u}_y=0$. No-slip and no penetration boundary were used on the wall. A pressure outlet boundary was imposed on the outlet.

RESULTS AND DISCUSSION

The experiments were performed for mixture flow rates Q_m ranging from 5 to 30 m^3/d and water cut α_w from 10% to 95% at four different pipeline inclinations (0°, +1°, +3° and +5°). The effects of flow rate, water cut and pipeline inclination on annular flow pattern, as well as holdup, slip ratio and pressure drop, were investigated.

1. Annular Flow Pattern

The annular patterns observed in the horizontal and slightly in-

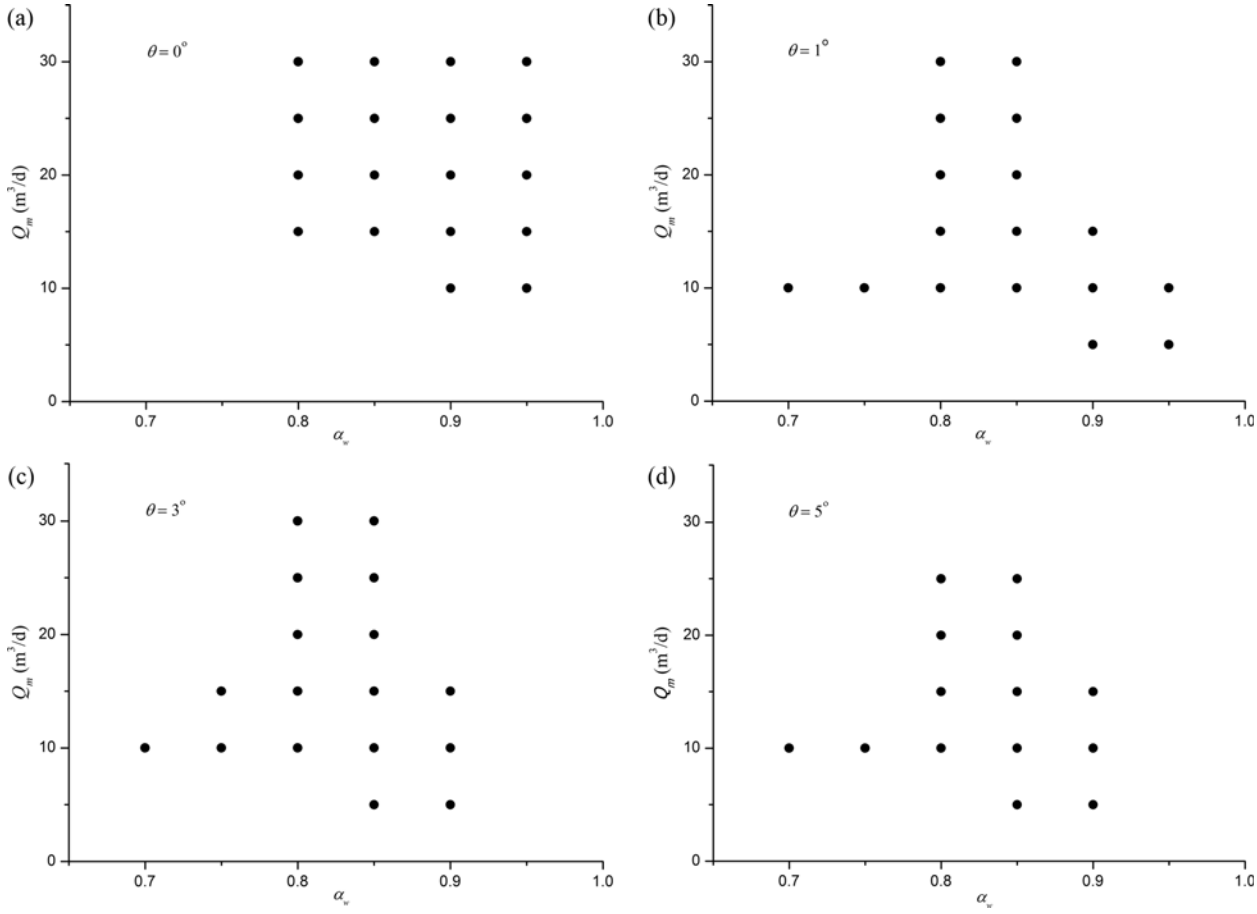

Fig. 5. The annular flow pattern in four inclination (a) θ=0°, (b) θ=+1°, (c) θ=+3° and (d) θ=+5°.

clined pipe are described here. The annular flow figures obtained in a horizontal and inclined pipe at Q_m=15 m^3/d and α_w=0.8 are shown in Fig. 4. It can be observed that the annular flow is eccentric, similar to findings other researchers obtained [23,36,37] due to gravity segregation. The oil-water interface is smooth at medium velocity. The oil layer thickness decreases as the pipe inclination increases, keeping the flow rate and water cut constant. This is because the component of gravity parallel to the pipe increased. Fig. 5 shows the annular flow pattern map at four pipe inclinations: θ=0°, +1°, +3° and +5°. It can be observed that the ranges for annular flow pattern in horizontal and inclined pipes are different. The annular flow in a horizontal pipe appeared with high water cut ($\alpha_w \geq 0.8$); at α_w=0.95, the flow pattern was observed in the range of Q_m from 10 to 30 m^3/d; but disappeared at Q_m=5 m^3/d.

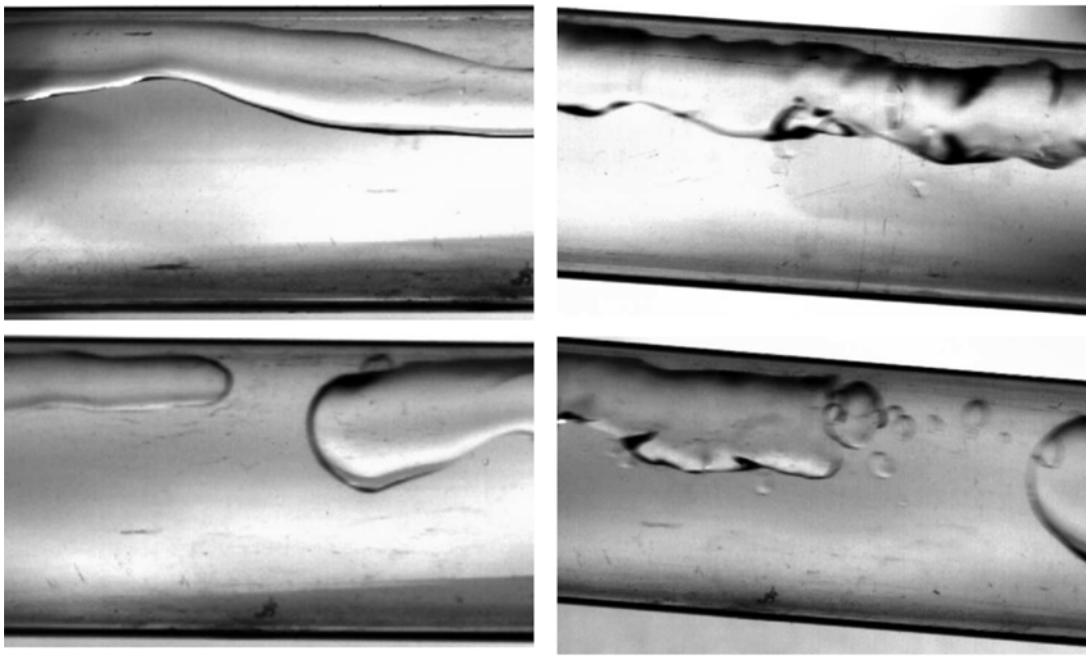

Fig. 6. The transition from annular flow to intermittent at Q_m=30 m^3/d and α_w=0.80 in (a) θ=0° and θ=+1° (b) θ=+3° and θ=+5° pipe.

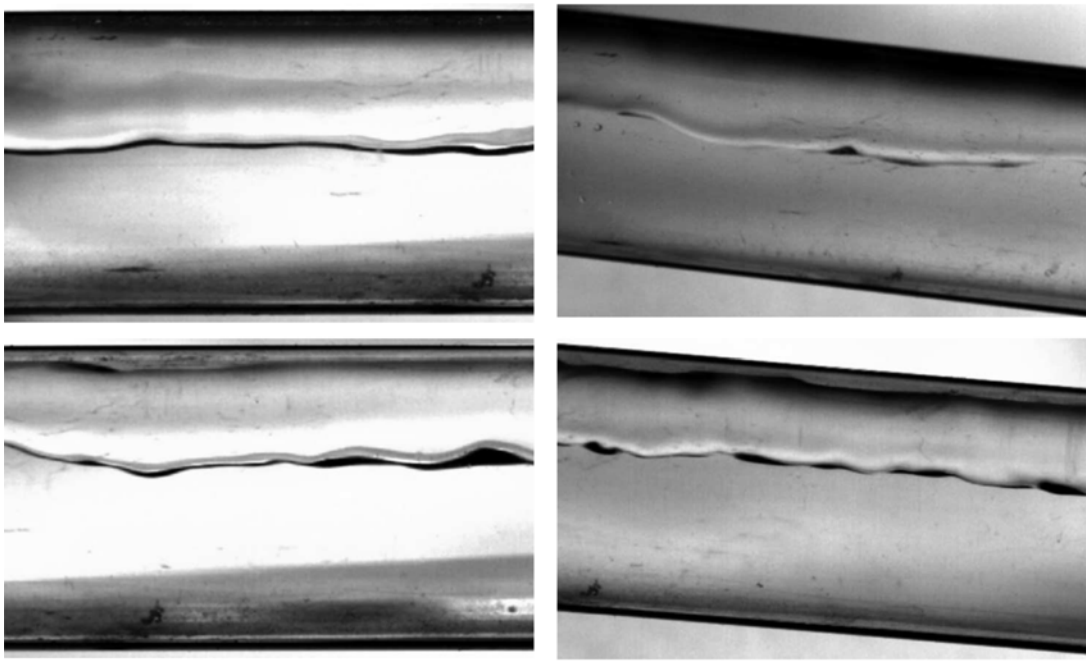

Fig. 7. The transition from annular flow to stratified flow at Q_m=20 m^3/d between α_w=0.70 and 0.80 in (a) θ=0° and (b) θ=+5° pipe.

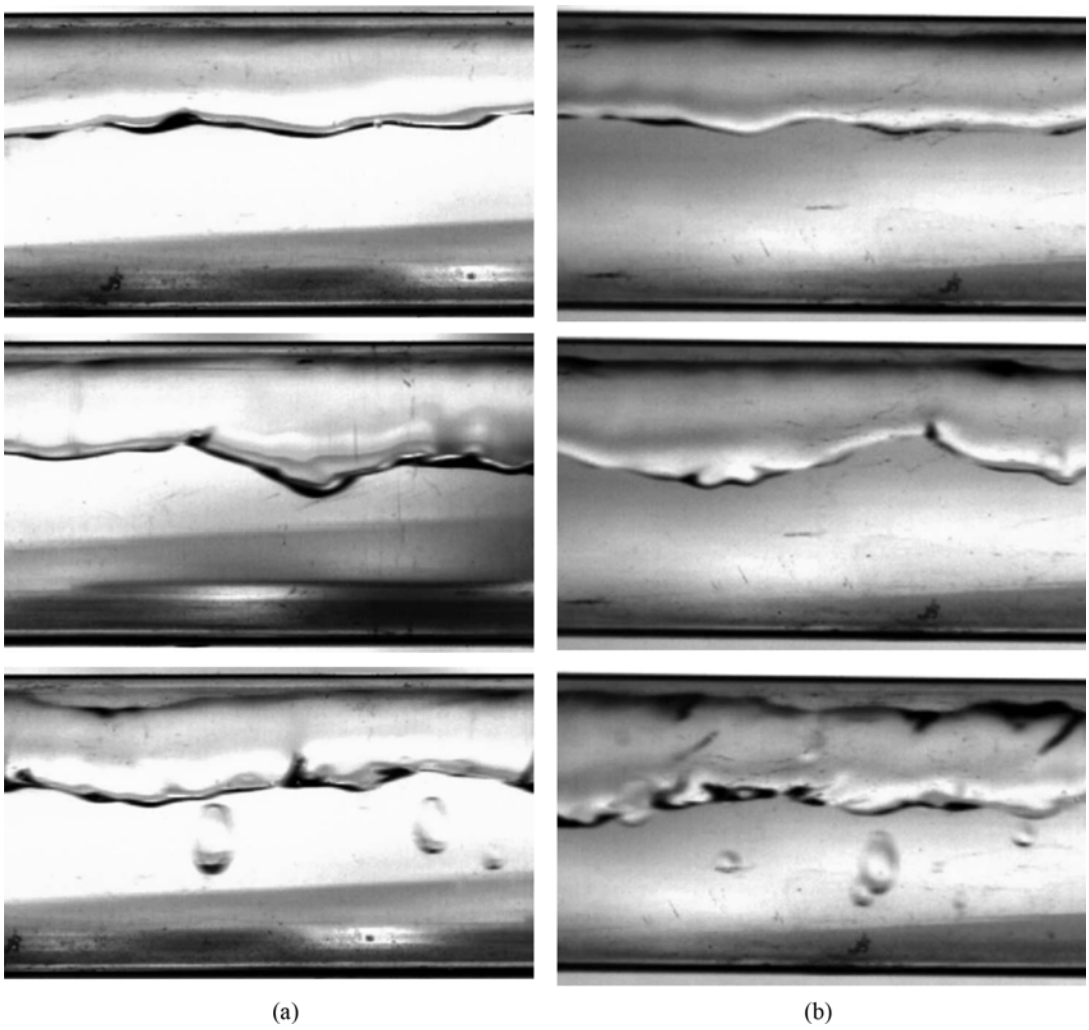

Fig. 8. Comparison of annular flow at and different Q_m (20, 25 and 30 m^3/d) in (a) θ=0° and (b) θ=+1° pipe.

Conversely, the annular flow patterns in inclined pipes are similar, in that at Q_m=10 m^3/d, the pattern appeared in the range of α_w from 0.7 to 0.9. In addition at a lower inlet flow rate (Q_m=5 m^3/d) the pattern was observed, but not for the horizontal pipe. The range of annular flow pattern is smaller than which obtained by Strazza et al. [23]. This means that the higher the viscosity of the oil, the more easily annular flow forms. Fig. 6 shows the transition from annular to intermittent. Keeping the water cut and flow rate constant, annular flow disappears as inclination increases. As be seen from Fig. 6(a), the inclination increased from 0° to +1°, the continuous oil layer transforms to an intermittent one, which is due to the gravitational forces overcoming the interfacial tension forces. A similar trend can be observed from Fig. 6(b) where the inclination changed from +3° to +5°.

The effects of inlet flow rate and water cut on annular flow pattern were also analyzed. When the oil cut increased, the oil layer became thicker and the interfacial tension pulled the interface up to the pipe [38,39]; thus, the upper water layer disappeared and the annular flow pattern changed to stratified flow (Fig. 7). Otherwise, if the water cut increases in inclined pipes, the oil layer changes to have intermittent attributes, because the interfacial tension forces are overcome by the gravitational force. The effect that flow rate has on annular flow is the appearance of an interfacial wave and oil droplets as flow rates increased [40]. Fig. 8 shows the annular flow at different flow rates; it can be observed that the interfacial waves and oil droplets appear one after another when the flow rates increase. Further observation shows that the oil-water interface in inclined pipes is smoother than in horizontal pipes at medium water cut.

2. Holdup

The in-situ oil holdup was measured by a ring impedance sensor to compare with those that were obtained from the CFD simulation results. Fig. 9 shows the phase distribution in the θ=+1° pipe cross section for various Q_m and α_w, where the solid black line indicates oil-water interface. It can be observed that the continuous oil layer cross section is almost round, so that the holdup can be calculated in accordance with a circular probe. The slip ratio S can be used to estimate the faster phase calculated as follows:

$$S = \frac{\alpha_o / \alpha_w}{\varepsilon_o / \varepsilon_w} \tag{12}$$

where ε is the in situ volume fraction; an S greater than 1 indi-

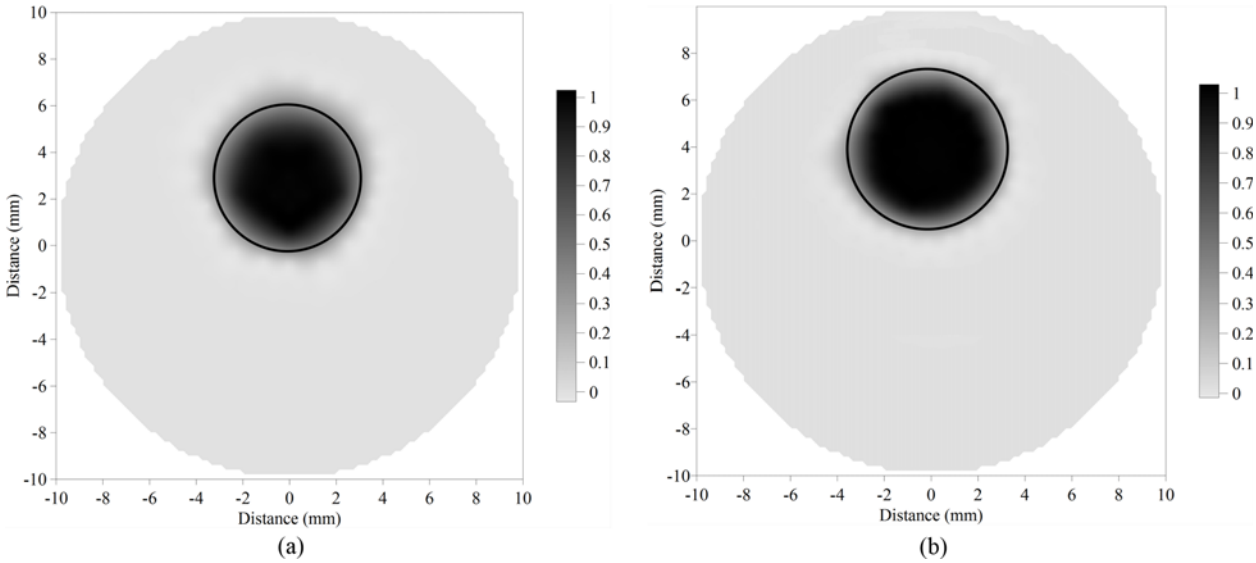

Fig. 9. Comparison distribution in θ=+1° pipe cross section at (a) Q_m=10 m³/d, α_w=0.90 and (b) Q_m=20 m³/d, α_w=0.80.

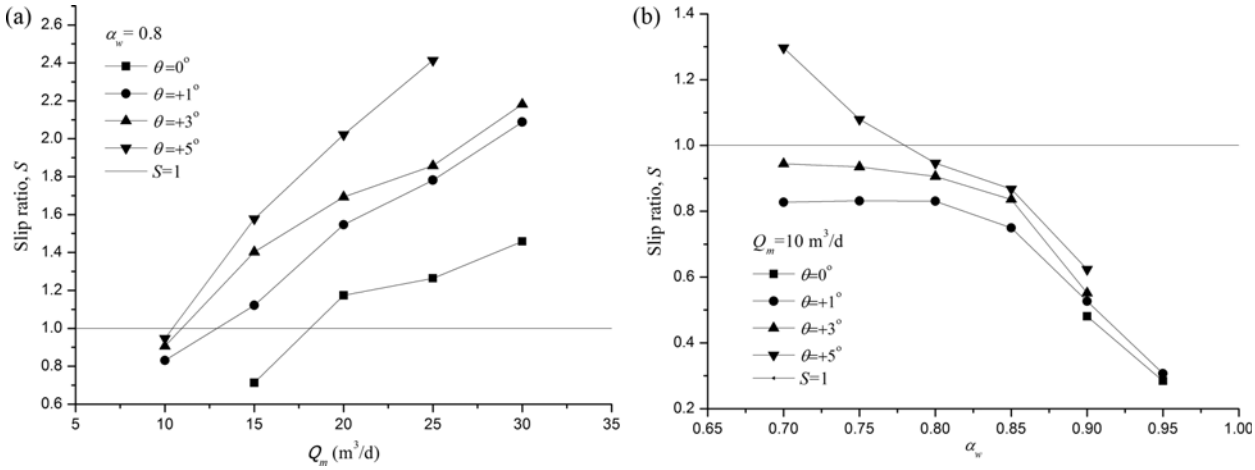

Fig. 10. The influence of (a) mixture flow rate (Q_m) and (b) input water cut (α_w) on the slip ratio of oil-water phase.

cates that the oil is the faster phase, and when S is less than 1, it indicates water flows faster than oil.

The influence of mixture flow rate and input water cut on the slip was investigated. The experimental results at different inclinations are shown in Fig. 10. At a constant input water cut (α_w=0.8), the slip ratios increased with increasing mixture flow rates at all of the inclinations (Fig. 10(a)). In addition, at a constant flow rate, the slip ratio increased with the pipe inclination increase. When annular flow was in the θ=+5° pipe, the slip ratio was greater than 1, which means the oil phase flowed faster than water; this was true at all of the flow rates in the inclined pipe. It can be observed from Fig. 10(b), that at a fixed constant flow rate, the slip ratio decreased as the input water cut increased; however, the rate of change increased with increasing α_w. This is because the oil layer was moving away from the central region of the pipe where the velocity was at a maximum as the water cut increased. In addition, at medium α_w values the inclination (θ) had an outstanding influence on slip ratio, which reduced with increasing α_w.

To evaluate the accuracy of the VOF model-predicted and experiment data, the results of the slip ratio obtained by model and experiment were compared by using the average relative error (e):

$$e = \frac{100}{n}\sum_{i=1}^{n}\left|\frac{S_{mod} - S_{exp}}{S_{exp}}\right|\% \quad (13)$$

The subscripts "mod" and "exp" denote VOF model prediction and experimental data, respectively; n is the number of experiments. Fig. 11 compares the VOF model's predicted values of slip ratio and the experimental data. As seen, a good agreement can be observed with all of the experiment data. The average relative errors slightly increased as the pipe inclination increased, and the maximum deviation was −17%, appearing at Q_m=25 m³/d and α_w=0.8 in the θ=+5° pipe. Moreover, the agreement was better as slip ratio became close to one. However, the VOF model under-predicted the slip ratio values when S>1.6.

3. Pressure Drop

The pressure drop measurements were performed at various

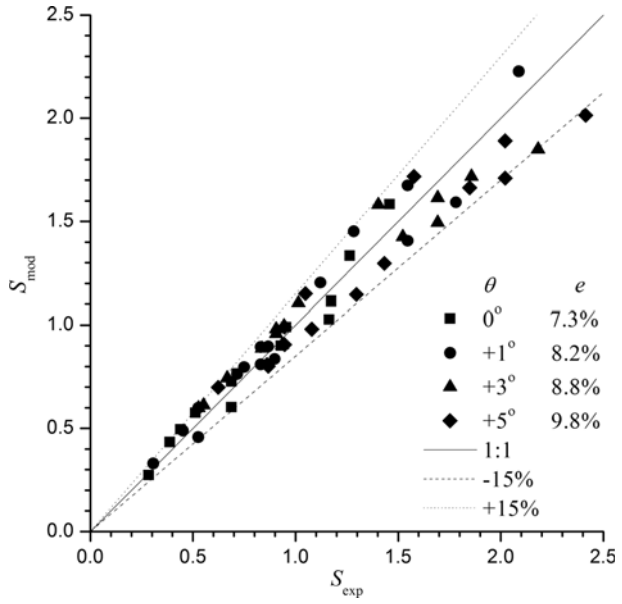

Fig. 11. The comparison of VOF predicted and experimental slip ratio.

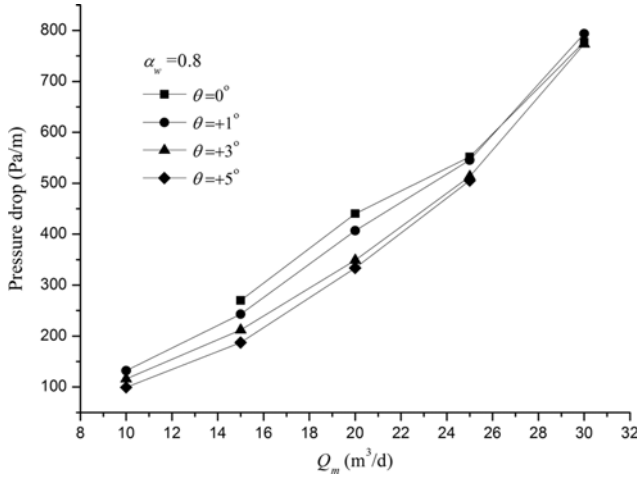

Fig. 12. Pressure drop of oil-water variation with mixture flow rate for four inclination at α_w=0.80.

flow rates and water cut in four inclinations; the results are in Figs.12 and 13. It is clear from Fig. 12 that the pressure drop at α_w=0.8 increased as flow rate increased in all of the inclinations. This is attributed to the increase in velocity leading to turbulence levels and Reynolds stress to increase significantly. Brauner [19] reported that the interfacial shear stress was proportional to the square of the core phase velocity. Keeping the flow rate at 10 m^3/d, the pressure drop increased with the water cut increase (Fig. 13) [41], which contributed to the rise of the average density of the mixture and led to an increase the pressure drop [42]. Furthermore, the pressure drop decreased as inclination increased when α_w<0.85. This may be due to the oil-water interface becoming smoother as water cut decreased. The change was more significant as the inclination increased.

Fig. 14 shows the VOF model prediction of pressure drop in

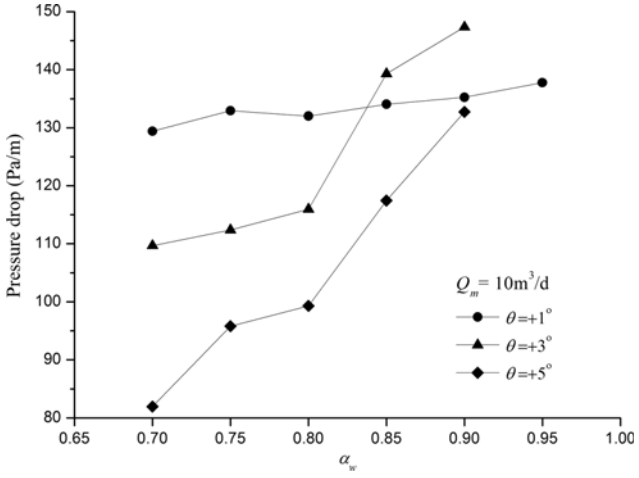

Fig. 13. Pressure drop of oil-water variation of water cut for three inclination at Q_m=10 m^3/d.

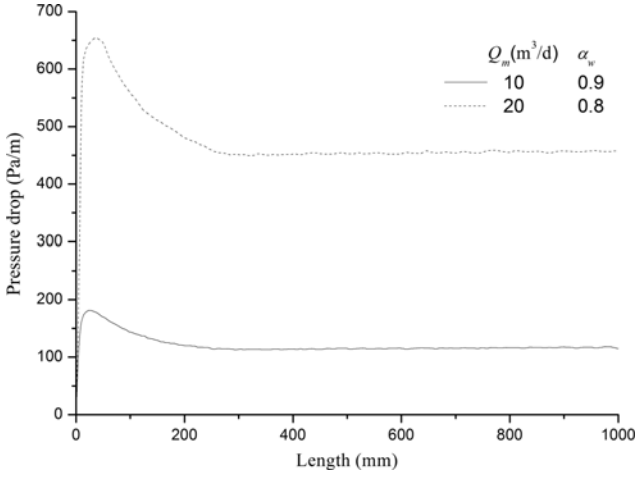

Fig. 14. Calculated pressure drop in horizontal pipe.

the horizontal pipe for two flow rates. The pressure drop increases rapidly from the inlet and reaches the maximum, then decreases gradually and tends to be stable with slight fluctuations. It is due to the velocity, which changes rapidly to approach the real velocity distribution near the inlet, whereas the velocity at the inlet boundary is assumed uniform. The length and fluctuation of the unsteady flow at Q_m=20 m^3/d is larger than the one at Q_m=10 m^3/d, which means the flow rate has more difficulty at larger flows in reaching stability. Thus, the pressure drop value is obtained at the stability section. Fig. 15 shows the comparison of predicted results and experimental data of the pressure drop. It can be observed that the pressure drop in all of the experimental data is less than 1,000 Pa/m. In addition, the VOF model shows very good agreement with the experimental results, especially when for a pressure drop larger than 400 Pa/m the maximum deviation is only ±10%. As the pressure drop is decreasing, the maximum deviation increases, especially when pressure drops less than 120 Pa/m which is about ±30%. In addition, the average deviation increases slightly with increasing inclination. This is due to smaller measured values having lower accuracy from the differential pressure transducer.

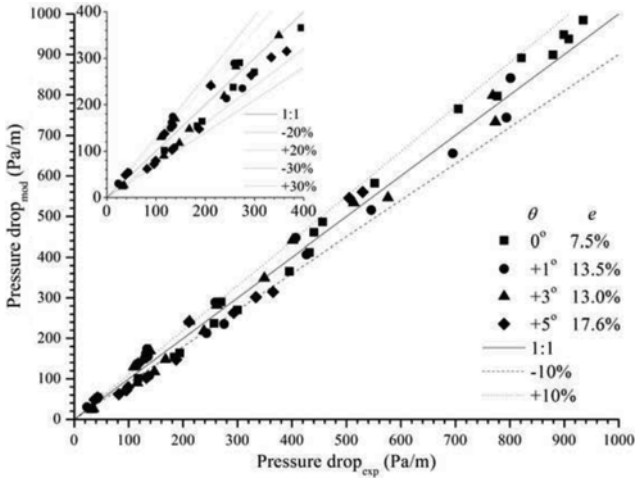

Fig. 15. Comparison of predicted results with experimental data of pressure drop.

CONCLUSIONS

The oil-water two-phase annular flow in horizontal and slightly inclined pipes with a small diameter was investigated both experimentally and numerically using the VOF model in considering the gravitation in flow direction with CFD software FLUENT 14.5. The following main conclusions were obtained:

(1) The annular flow pattern is influenced by inlet flow rate, water cut and pipe inclination. The upper water layer surrounding the oil layer disappears as the water cut decreases due to the interfacial tension pulling the interface up the pipe. When the flow rate increases, interfacial waves appear and lead to the appearance of oil droplets. The oil layer is discontinuous with the pipe inclination increasing at high water cut due to the gravity force being larger than the surface tension force; thus, the range of flow pattern in an inclined pipe is smaller than that in a horizontal pipe.

(2) The slip ratio increases with increasing inlet flow rate at all inclinations; moreover, the increase at a high inclination is more rapid than that at a low inclination. At high water cut, the slip ratio speedily decreases as water cut increases in the θ=0°, +1° and +3° pipe; however, in the θ=+5° pipe, the slip ratio changes quickly with inlet flow rate and water cut change.

(3) Pressure drop increases sharply with increasing flow rate in all of inclinations. In addition, pressure drop increases with respect to the decrease in water cut, which is more pronounced at high inclination than at lower inclination.

(4) The VOF model considering gravitation flow direction has been utilized to calculate the oil-water two-phase annular flow in horizontal and slightly inclined pipes. Good agreement was obtained between the predicted results and experimental data. The deviation of pressure drop results between experimental and numerical values demonstrates that the modified VOF model can predict characteristics of annular flow in horizontal and slightly inclined pipes.

ACKNOWLEDGEMENT

The financial support for this study provided by the National Science Foundation of China (41374116) is gratefully acknowledged.

REFERENCES

1. A. L. Cox, University of Texas at Austin (1985).
2. N. Brauner and D. Moalem Maron, *Int. J. Multiphase Flow*, **18**. 123 (1992).
3. J. L. Trallero, in *Discipline of Petroleum Engineering*, University of Tulsa, 176 (1995).
4. A. Beretta, et al., *Int. Commun. Heat Mass Transf.*, **24**, 223 (1997).
5. P. Angeli and G. F. Hewitt, *Int. J. Multiphase Flow*, **26**, 1117 (2000).
6. G. Elseth, Norwegian University of Science and Technology, 270 (2001).
7. D. R. Chakrabarti, G. Das and S. Ray, *Chem. Eng. Technol.*, **28**, 1003 (2005).
8. T. Al-Wahaibi, et al., *J. Petroleum Sci. Eng.*, **122**, 266 (2014).
9. O. M. H. Rodriguez and R. V. A. Oliemans, *Int. J. Multiphase Flow*, **32**, 323 (2006).
10. J. Y. L. Lum, T. Al-Wahaibi and P. Angeli, *Int. J. Multiphase Flow*, **32**, 413 (2006).
11. W. A. S. Kumara, B. M. Halvorsen and M. C. Melaaen, *Chem. Eng. Sci.*, **65**, 4332 (2010).
12. G. Ooms, *Appl. Sci. Res.*, **26**, 147 (1972).
13. R. V. A. Oliemans and G. Ooms, *Core-Annular Flow of Oil and Water through a Pipeline*, in *Multiphase Science and Technology*, G. F. Hewitt, J. M. Delhaye and N. Zuber, Ed., Springer Berlin Heidelberg, 427 (1986).
14. M. S. Arney, et al., *Int. J. Multiphase Flow*, **19**, 1061 (1993).
15. R. Bai, K. Kelkar and D. D. Joseph, *J. Fluid Mechanics*, **327**, 1 (1996).
16. D. D. Joseph, et al., *Annual Review of Fluid Mechanics*, **29**, 65 (1997).
17. D. Barnea, *Int. J. Multiphase Flow*, **12**, 733 (1986).
18. D. Barnea and Y. Taitel, *Chem. Eng. Sci.*, **44**, 325 (1989).
19. N. Brauner, *Int. J. Multiphase Flow*, **17**, 59 (1991).
20. A. C. Bannwart, *J. Petroleum Sci. Eng.*, **32**, 127 (2001).
21. O. M. H. Rodriguez and A. C. Bannwart, *AIChE J.*, **54**, 20 (2008).
22. O. M. H. Rodriguez, A. C. Bannwart and C. H. M. de Carvalho, *J. Petroleum Sci. Eng.*, **65**, 67 (2009).
23. D. Strazza, et al., *Chem. Eng. Sci.*, **66**, 2853 (2011).
24. T. Ko, et al., *Int. J. Multiphase Flow*, **28**, 1205 (2002).
25. S. Ghosh, G. Das and P. K. Das, *Chem. Eng. Processing: Process Intensification*, **49**, 1222 (2010).
26. V. V. R. Kaushik, et al., *J. Petroleum Sci. Eng.*, **86-87**, 153 (2012).
27. J. O. McCaslin and O. Desjardins, *Int. J. Multiphase Flow*, **67**, 88 (2014).
28. S. Tripathi, et al., *Procedia IUTAM*, **15**, 278 (2015).
29. S. Ghosh, G. Das and P. K. Das, *Chem. Eng. Res. Design*, **89**, 2244 (2011).
30. F. Jiang, et al., *Ind. Eng. Chem. Res.*, **53**, 8235 (2014).
31. S. Ghorai and K. D. P. Nigam, *Chem. Eng. Processing: Process Intensification*, **45**, 55 (2006).
32. S. C. K. De Schepper, G. J. Heynderickx and G. B. Marin, *Chem. Eng. J.*, **138**, 349 (2008).
33. J. Brackbill, D. B. Kothe and C. Zemach, *J. Comput. Phys.*, **100**, 335 (1992).
34. M. R. Rampure, V. V. Buwa and V. V. Ranade, *Can. J. Chem. Eng.*,

81, 692 (2003).
35. R. M. A. Masood and A. Delgado, *Chem. Eng. Sci.*, **108**, 154 (2014).
36. B. Grassi, D. Strazza and P. Poesio, *Int. J. Multiphase Flow*, **34**, 950 (2008).
37. P. Poesio, D. Strazza and G. Sotgia, *Appl. Thermal Eng.*, **49**, 41 (2012).
38. T. S. Ng, C. J. Lawrence and G. F. Hewitt, *Int. J. Multiphase Flow*, **27**, 1301 (2001).
39. T. S. Ng, C. J. Lawrence and G. F. Hewitt, *Chem. Eng. Res. Design*, **82**, 309 (2004).
40. T. Al-Wahaibi and P. Angeli, *Int. J. Multiphase Flow*, **37**, 930 (2011).
41. J. Y. L. Lum, J. Lovick and P. Angeli, *Can. J. Chem. Eng.*, **82**, 303 (2004).
42. F. Jiang, et al., *Chem. Eng. Technol.*, **37**, 659 (2014).